Title

c-Axis-Oriented Platelets of Crystalline Hydroxyapatite in Biomimetic Intrafibrillar Mineralization of Polydopamine-Functionalized Collagen Type I.

Journal

ACS Omega, 7(6)

Authors

Amornkitbamrung, Urasawadee
In, Yongjae
Wang, Zhen
et al.

Publication Date

2022-02-15

DOI

10.1021/acsomega.1c05198

Peer reviewed

ACS OMEGA

http://pubs.acs.org/journal/acsodf

Article

c-Axis-Oriented Platelets of Crystalline Hydroxyapatite in Biomimetic Intrafibrillar Mineralization of Polydopamine-Functionalized Collagen Type I

Urasawadee Amornkitbamrung, Yongjae In, Zhen Wang, Jiyoon Song, Sang Ho Oh,* Min-Ho Hong,* and Hyunjung Shin*

Cite This: *ACS Omega* 2022, 7, 4821−4831

Read Online

ACCESS | Metrics & More | Article Recommendations | Supporting Information

ABSTRACT: Mineralized collagen fibrils are important basic building blocks of calcified tissues, such as bone and dentin. Polydopamine (PDA) can introduce functional groups, i.e., hydroxyl and amine groups, on the surfaces of type I collagen (Col-I) as possible nucleation sites of calcium phosphate (CaP) crystallization. Molecular bindings in between PDA and Col-I fibrils (Col-PDA) have been found to significantly reduce the interfacial energy. The wetting effect, mainly hydrophilicity due to the functional groups, escalates the degree of mineralization. The assembly of Col-I molecules into fibrils was initiated at the designated number of collagenous molecules and PDA. In contrast to the infiltration of amorphous calcium phosphate (ACP) precursors into the Col-I matrix by polyaspartic acid (pAsp), this collagen assembly process allows nucleation and ACP to exist in advance by PDA in the intrafibrillar matrix. PDA bound to specific sites, i.e., gap and overlap zones, by the regular arrangement of Col-I fibrils enhanced ACP nucleation and thus mineralization. As a result, the *c*-axis-oriented platelets of crystalline hydroxyapatite in the Col-I fibril matrix were observed in the enhanced mineralization through PDA functionalization.

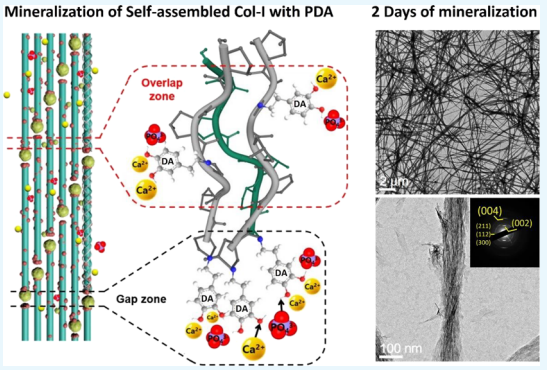

1. INTRODUCTION

Collagen is one of the main components of extracellular matrices in human and animal bodies. It plays several important roles in terms of mechanical resilience for connective tissues and supporting cell growth. Type I collagen (Col-I) is the most abundant collagen type as it is the main organic substance of the hard tissue, e.g., bone and dentin, in vertebrates. Mineralized Col-I fibrils are one of the critical components in natural bone formation as the collagen molecules assembled into fibrils and mineralized via the formation of crystalline plates in the form of hydroxyapatite (HAp) nanocrystals. Mineralized Col-I fibrils by HAp nanocrystals provide mechanical support. The presence of mineralized HAp provides enough strength and toughness in bone tissue compared with a tropocollagen molecule alone as the nanoscale structure of mineralized building blocks. In Col-I fibrils, $Ca_3(PO_4)_{2n}$ clusters, known as Posner's clusters, are nucleated close to the C-terminal of collagen molecules and then grow by further mineral deposition.[1−3] This spatial constraint and framework lower the energy barrier, resulting in the structure of platelet-like HAp crystals at 37 °C.[4] Over the past decades, many research groups have been studying to understand the mechanisms of collagen mineralization. The structure of mineralized collagen was determined by small-angle X-ray and neutron diffraction studies, which showed that HAp crystals were regularly deposited within the Col-I fibrils.[5,6] A definitive proof of these results was reported earlier by Robinson and Watson through an electron microscopy study in 1952.[7] Since then, studies on bone tissue analysis by transmission electron microscopy (TEM) have been steadily progressing and have had a great impact on the theory of nucleation and inorganic crystal growth *in vivo*.[8−11] In recent TEM studies, the mineralization process in collagen matrices has been also analyzed and interpreted based on the nonclassical theory of crystallization. The nonclassical theory began with the observation of an amorphous precursor followed by the concept of multistage crystallization initially proposed by Ostwald.[12] One example of such a mineral is calcium phosphate (CaP), and early research indicated the existence of a metastable amorphous precursor phase that is assumed to be composed of $Ca_9(PO_4)_6$.[13] Amorphous calcium phosphate (ACP) is released from cells during bone formation,

Received: September 19, 2021
Accepted: January 6, 2022
Published: February 7, 2022

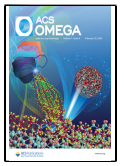

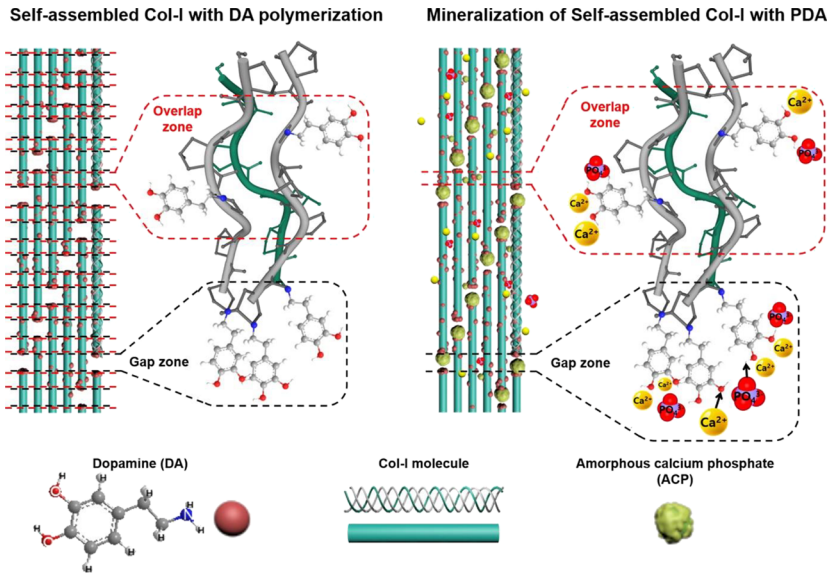

Figure 1. Schematic of PDA-assisted mineralization with Col-I fibrillation. DA molecules added during the Col-I self-assembly process were chemically bound to the surface of Col-I molecules in addition to the gap and overlap zones that exist between Col-I molecules in fibrils. In addition, it is hypothesized in this study that PDA chemically bound to several sites inside the fibrils attracts Ca^{2+} and PO_4^{3-} ions for mineralization, thereby affecting ACP nucleation and intrafibrillar mineralization.

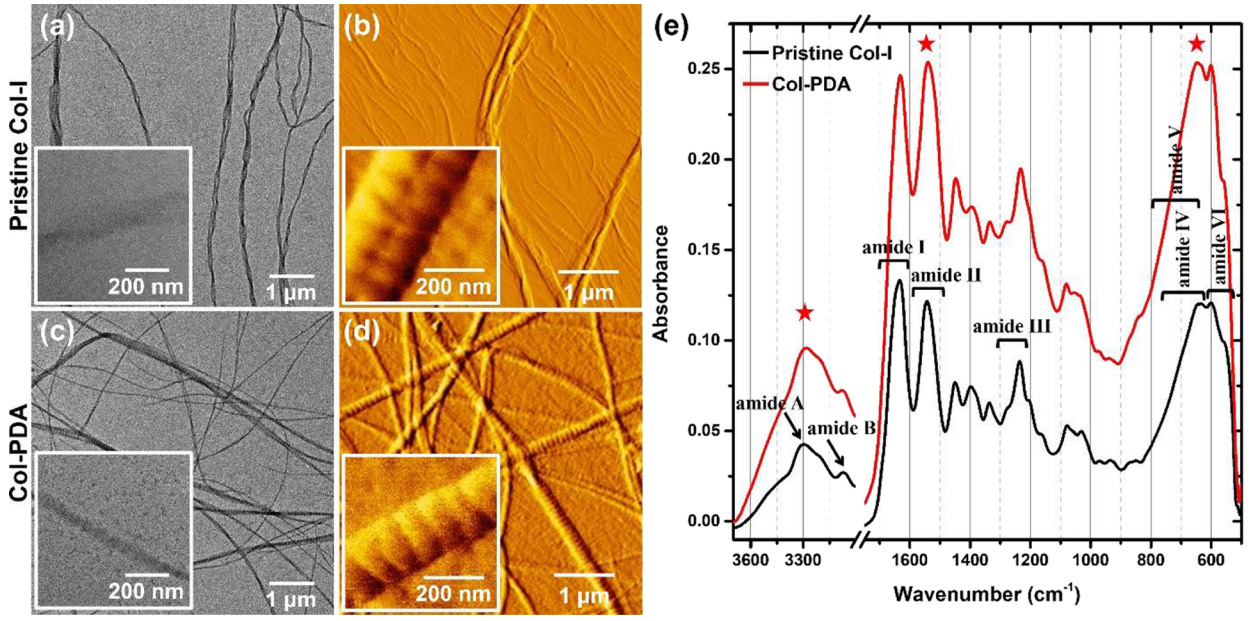

Figure 2. Self-assembled Col-I and PDA-Col fibrils. (a, c) TEM images of pristine Col-I and Col-PDA (fibrillation with a Col-I and DA mass ratio of 5:16). The inset images are the high-magnification TEM images of pristine Col-I and Col-PDA fibrils without negative staining. However, the Col-PDA fibrils relatively exhibit the dark/bright pattern of a well-ordered structure compared to pristine Col-I fibrils. It can be inferred that this difference is due to DA polymerization at a specific area of Col-I fibrils. (b, d) AFM images show that the self-assembled pristine Col-I and Col-PDA fibrils on the mica substrate are less than 1 μm in diameter and are aligned to the length of the micrometer scale. The inset images are high-magnification AFM images clearly showing the *d*-band characteristic of self-assembled Col-I fibrils. (e) FTIR results of self-assembled pristine Col-I and Col-PDA fibrils. Specific peaks from the catechol group in PDA are marked with stars.

develops into crystalline HAp in 40 nm gaps present in the Col-I fibrils, and have their *c*-axis aligned parallel to the long axis of fibrils.[14−17] It is widely known that in nature, the biomineralization of collagen is regulated by acidic non-collagenous proteins (NCPs). In Col-I fibrils, the positive net charges at the gap zone are believed as the preferred sites for mineral nucleation, which then further extends crystals along microfibrillar collagen spaces. The polyanionic polymers, such as polyaspartic acid (pAsp), have been researched and commonly used as the sequestration analogues of NCPs. They also stabilize the ACP precursors and hence facilitate intrafibrillar mineralization.[18−21] The negatively charged pAsp promotes the infiltration by forming the pAsp-ACP complex and is delivered to the positive net charged gap zone by the attraction and attained intrafibrillar mineralization.[16]

To increase the degree of mineralization, which leads to better mechanical and osteoconductive properties than Col-I fibrils alone,[22] extensive research works have been performed

https://doi.org/10.1021/acsomega.1c05198
ACS Omega 2022, 7, 4821−4831

on the mineralization by introducing additional functional groups on collagen matrices. The functional groups such as in citric acid and polydopamine (PDA) including carboxylic acid, hydroxyl, and amine on the surfaces of collagen matrices were introduced as possible nucleation sites.[23,24] The reduction of interfacial energy between collagen and mineralized calcium phosphate can enhance mineralization and improve the mechanical properties of mineralized organic and inorganic composites.[24,25] PDA is well known for its hydrophilicity due to the hydroxyl and amino groups of its molecules.[26] Hence, PDA has earned interest for surface modification in many studies, especially as a key approach to incorporate new functionalities into existing biomaterials. PDA coatings have also been exploited and identified to show an excellent biocompatibility with improved cell attachment, proliferation, and a good adhesion of fibroblasts.[27] The composite nanolayers of CaP and PDA were reported to significantly enhance surface roughness and hydrophilicity, stimulating the attachment, proliferation, alkaline phosphatase activity, and bone-related gene expression of human bone marrow stromal cells.[28] PDA-coated HAp was shown to increase the osteogenesis and angiogenesis of human mesenchymal stem cells (hMSCs), which was proven to increase the focal adhesion kinase level as the amount of PDA increased and enhance the cell attachment.[29] PDA, which is regarded as a surface modifier and is constantly used to modify the surface of biomaterials, is known to bind to calcium ions.[30] It has also been proven to accelerate the crystallization of HAp by promoting mineralization in the collagen matrix of the dentine by exerting the advantage of the presence of a rich catecholamine motif.[24] It can be very attractive to mineralization in the process of Col-I fibrosis, which is composed of a major component in bone tissue among skeletal tissues.

Herein, we report that the intrafibrillar mineralization can be enhanced by the integration of PDA in Col-I fibrils. The molecular structure of PDA provides abundant negative charges, which were introduced as possible nucleation sites of crystallization of CaP with Ca^{2+} and PO_4^{3-} ions by reducing the interfacial energy. The effect of PDA on mineralization by an *in vitro* model was studied compared with the pristine Col-I fibrils. Nucleation and growth of HAp crystals proceeded at regular and defined locations of Col-I fibrils, especially intrafibrillar regions, and it was demonstrated that the HAp crystals are oriented with their *c*-axis parallel to the direction of the collagen molecular structure. In this study, we focus on the efficiency of PDA for the nucleation and growth of HAp crystals during intrafibrillar mineralization, as shown in Figure 1.

2. RESULTS AND DISCUSSION

Self-assembly of Col-I fibrils was carried out in buffer solution at 37 °C with and without PDA. The self-assembled Col-I fibrils with a diameter of less than 1 μm, as expected, were clearly observed by TEM and atomic force microscopy (AFM), as shown in Figure 2a−d. The TEM images of pristine Col-I and Col-PDA (fibrillation by a mass ratio of Col-I and dopamine (DA) of 5:16) are shown in Figure 2a,c, respectively. The insets are higher-magnification TEM images. Col-PDA fibrils exhibited clearer dark/bright patterns of a well-ordered structure than pristine Col-I fibrils even though both fibrils were not negatively stained for TEM imaging, as shown in Figure 2c. It can be inferred that DA polymerization occurs at a specific area of Col-I fibrils. As shown in Figure S1, a typical banding pattern of approximately ∼67 nm was clearly observed. The self-assembled Col-I fibrils in Figure S1 were negatively stained by using uranyl acetate before observing by TEM. AFM images showed that the self-assembled pristine Col-I and Col-PDA fibrils on the mica substrates are also less than 1 μm in diameter and are aligned to the length of the micrometer scale, as shown in Figure 1b,d, respectively. Inset images in both Figure 1b,d are higher-magnification AFM images clearly showing the *d*-band characteristic of self-assembled Col-I fibrils. AFM analysis revealed that the reconstituted fibrils were several micron-meters long and 50−100 nm wide and a typical banding pattern with around 67 nm periodicity was found in both Col-I and Col-PDA fibrils. It is confirmed that the Col-I molecules were well assembled into fibrils with a staggered structure of Col-I molecules, creating the gaps and overlapping patterns. The microfibrils of Col-I, as shown in Figure 2b, which are the initial fibrils, are likely to be aligned and guided by the underlying mica as a substrate. The alignment mechanism of micro-Col-I fibrils on mica is caused by the interaction between the fibrils and highly charged and chemically rich surfaces in mica substrates.[31]

In the collagen self-assembly process, the ratio of Col-I and DA molecules has been optimized where DA does not affect the collagen fibrillar structure. Figure S2 shows the change in Col-I fibrils' morphology with a different amount of DA. With low amounts of DA (Col-I:DA = 5:4, 5:8, 5:16, and 1:8), the results of AFM analysis indicated that the self-assembled Col-I fibrils' incorporation with PDA, as shown in Figure S2, was successfully formed with the original characteristic morphology of Col-I fibrils as compared with the self-assembled collagen ones without DA (see Figure 2b). In the collagen self-assembly process, when higher concentrations of DA were applied (Col-I:DA = 1:16 and 1:32), the Col-I fibrils showed an irregular shape and appeared to be disintegrated. It is suggested that the extensive self-polymerization of DA can delay the self-assembly of collagen molecules, resulting in Col-I fibrils with unusual morphologies. Based on this result, a group that had the ratio of Col-I and DA synthesized at 5:16 was chosen, as shown in Figure 2c,d, now referred to as Col-PDA, and further experiments were performed. In the low-magnification TEM and AFM images, Col-PDA fibrils are more rigidly aligned than pristine Col-I fibrils. The self-assembly process of Col-I fibrils takes advantage of the like-charge attraction generated by the counterions, which screen the repulsive electrostatic forces between monomers and allow short-range attractive forces to act.[32] Based on this mechanism, PDA can serve as a bridge within the excess charged regions of fibrils and plays a dominant role in Col-I alignment during fibrillation.

One of the important criteria for Col-I fibrils' modification is that the secondary structure (i.e., combination of hinge-like glycine and hydroxyproline units to lead to helical macromolecules) of Col-I molecules after the modification by PDA should not be disintegrated. The CD and FTIR spectra of Col-I fibrils after incorporating PDA (Col-PDA) were measured and analyzed. The interaction of PDA and Col-I was confirmed by FTIR spectroscopy, as shown in Figure 2e. In self-assembled Col-I, chemically bound molecules, i.e., repeating units of polypeptides and proteins, generate characteristic IR absorption bands, for example, amides A, B, and I−VII. The amide I (1690−1600 cm^{-1}) and II (1575−1480 cm^{-1}) bands are the most conspicuous vibrational bands, and the amide I band is known to be the most sensitive spectral region to protein secondary structural components due to the C═O

https://doi.org/10.1021/acsomega.1c05198
ACS Omega 2022, 7, 4821−4831

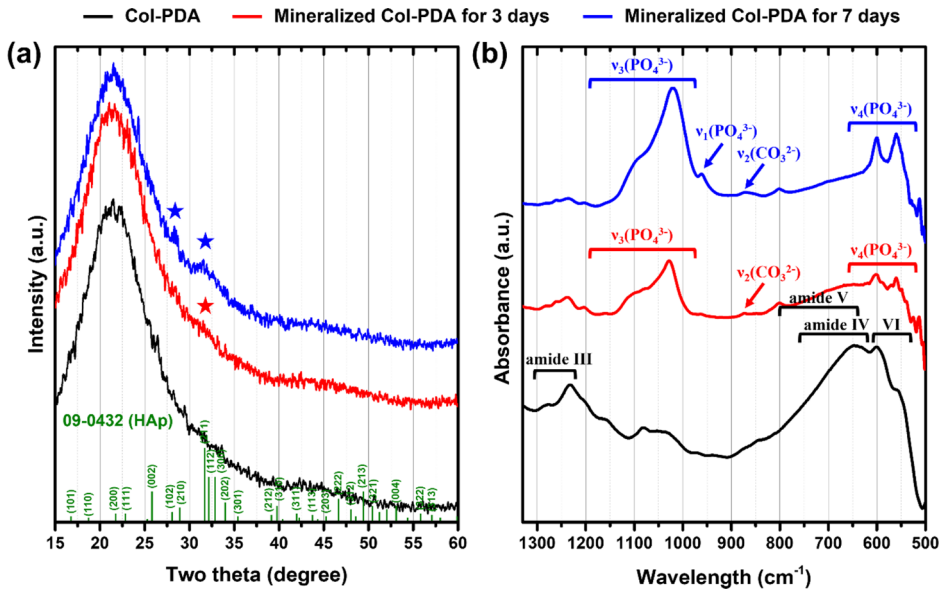

Figure 3. (a) XRD patterns of the mineralized Col-PDA fibrils for 3 (red solid line) and 7 (blue solid line) days. The XRD pattern of the unmineralized Col-PDA fibrils is the control (black solid line). The merged diffraction lines (28−29 and 31−33°) are marked with stars in mineralized Col-PDA fibrils. (b) FTIR spectra of the mineralized Col-PDA fibrils for 3 (red solid line) and 7 (blue solid line) days. The FTIR spectrum of the unmineralized Col-PDA fibrils is the control (black solid line).

stretch vibrations of about 80% peptide linkages. The amide II band originates from 40−60% of the in-plane NH bending and 18−40% of the CN stretching vibration and has a relatively lower protein structural sensitivity than amide I.[33,35] The remaining amide vibration bands are complex depending on the force field, side chains, and hydrogen bonding properties, making them less useful for protein structural studies. In general, amide A (3300 cm^{-1}) and B (3100 cm^{-1}) bands are mainly due to the NH stretching vibration, and it is inferred that the broadening of this area as a result of Col-PDA is due to the intermolecular hydrogen bonds of the catechol group formed between Col-I and PDA with OH.[34,35] The absorbance of amide II, which has a relatively high proportion of the NH bending vibration compared to amide I, exhibited a higher value due to the overlapping of the existing NH bending by hydrogen bonding of the PDA catechol group. In addition, it can be explained in accordance with the result that the out-of-plane NH bending in amide V (800−640 cm^{-1}) was also influenced by the catechol group of PDA so that the absorbance of Col-PDA showed a relatively higher intensity than that of pristine Col-I.[35−37] It is confirmed that there is no change in the native triple-helical structure of Col-I molecules after the incorporation of PDA. As shown in Figure S3, a typical CD spectrum of triple-helical Col-I molecules was characterized by an amplitude in the positive direction at 222 nm followed by a relatively negative minimum at 197 nm. The self-assembled Col-PDA also showed the same results as the pristine Col-I molecules in the analogous wavelength range. The difference in CD intensity was caused by the effect of aggregation and precipitation of Col-I fibrils by self-assembly.

A modified simulated body fluid (m-SBF) with pAsp as prepared in the Experimental Section was used as a medium for intrafibrillar mineralization. The XRD patterns and FTIR spectrum in Figure 3 showed the presence of crystalline HAp for the pristine Col-PDA (in black) as a control and for the 3 (in red) and 7 (in blue) days of mineralization. The patterns showed the extensive broad peak in the two theta range of 10−35°, which is a typical pattern of Col-I, as shown in Figure 3a.[38] A diffraction peak appeared from the third day of mineralization of Col-PDA fibrils, with the position of the peak at 31−33° corresponding to interplanar spacings of (211), (112), and (300) in crystalline HAp (ICDD 09-0432). Li et al. reported that the synthetic HAp crystals *in vivo* had a higher crystallinity and more distinct characteristic peaks than the bone apatite crystals from the rabbit femur, showing an envelope curve of HAp diffraction with less crystallization.[39] As the XRD result of real bone apatite crystals showed peaks at 28−29° [(102) and (210)], the result of Col-PDA after 7 days of mineralization also showed the peaks at the same diffraction angle. However, it should be noted that the obtained XRD peaks at 31−33° from Figure 3a are less sharp and broad even up to 8 days of mineralization, as shown in Figure S7. The broad peak from XRD indicates crystals that are small in size and poorly crystalline, which contradicts the results of selected area electron diffraction (SAED) in HRTEM that will be shown and discussed in later. FTIR analysis was used to further characterize the chemical composition of the mineralized Col-PDA fibrils (Figure 3b). In the mineralized Col-PDA fibrils, phosphate (1190−976, 961, and 660−520 cm^{-1}) and carbonate (873 cm^{-1}) bands were found along with the peaks of the amide bands as in the Col-I fibrils, which can infer that the mineralized Col-PDA fibrils are like the bone tissue. Unlike synthetic HAp, mineralized Col-PDA fibrils, like bone apatite, exhibit a higher CO_3^{2-} content over time. The CO_3^{2-} group occupies the −OH group position of the HAp structure, and it can be deduced that the small molecules constituting the Col-I molecules and PDA composed of H, C, N, and O may be included in the apatite lattice during mineralization. As a result, the resulting mineralized Col-PDA fibrils in m-SBF can be considered as biomimetic mineralization.

The complete mineralization states of pristine Col-I and Col-PDA were demonstrated with a series of mineralization times, 0.5, 1, 3, 5, and 7 days, in m-SBF, as shown in Figure 4a−j. The pristine Col-I fibrils without PDA were used as

https://doi.org/10.1021/acsomega.1c05198
ACS Omega 2022, 7, 4821−4831

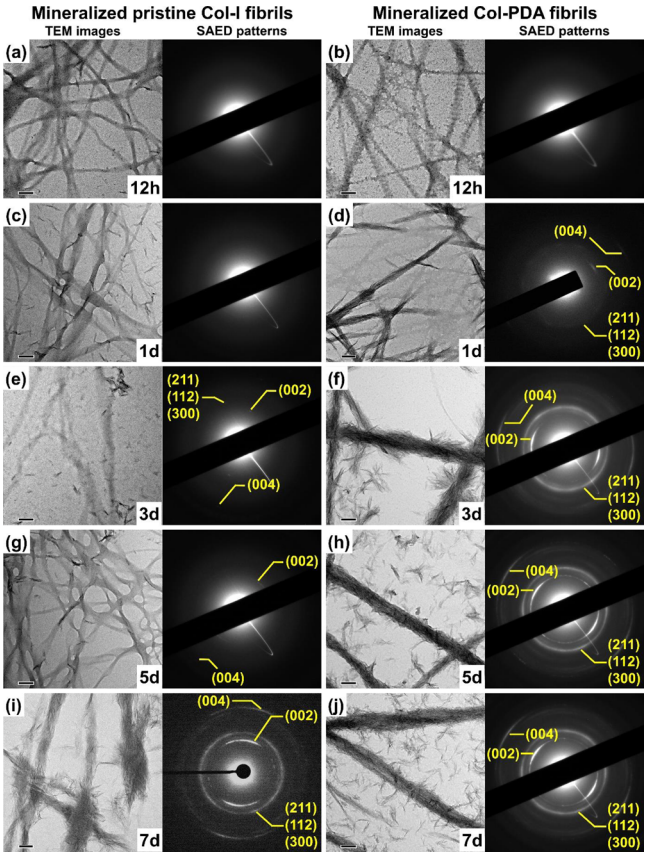

Figure 4. Bright-field TEM images and corresponding SAED patterns of the mineralized (a, c, e, g, i) pristine Col-I fibrils and (b, d, f, h, j) Col-PDA fibrils (scale bars: 200 nm). The self-assembled Col-I and Col-PDA fibrils were incubated in m-SBF for (a, b) 12 h, (c, d) 1 day, (e, f) 3 days, (g, h) 5 days, and (i, j) 7 days. (a, c, e) The intrafibrillar mineralization of the pristine Col-I fibrils after incubating in m-SBF for up to 3 days at 37 °C failed. Corresponding SAED patterns showed no mineralization. (d) Col-PDA fibrils were partially mineralized after a day. (f, h, j) Col-PDA fibrils underwent full intrafibrillar mineralization after 3 days. The SAED patterns of minerals in Col-PDA fibrils matched with crystalline HAp.

controls in Figure 4a,c,e,g,i. As shown in Figure 4a, no banding patterns are observed in the early mineralization stage of 0.5 day, while Col-PDA fibrils in Figure 4b still retained the banding patterns. The dark-field images are formed by collecting scattered electrons with an annular dark-field detector. The higher intensity results from scattering of the heavier elements, leading to atomic number (z) contrast.[40] It can be assumed that the z-contrast of the banding pattern that is found in Col-PDA was evidence of Ca and P that infiltrated in the gap since they are heavier than carbon (see Figure 4b). The EDS mapping of Col-PDA indicated the distribution of Ca and P elements that are found at the fibril area, ascribing to the fact that the minerals infiltrated into the fibrils at the early state of mineralization (see Figure S4). The mineralization rate of pristine Col-I fibrils was significantly slower than that of Col-PDA fibrils, which was indicated by the less electron-dense TEM images (Figure 4a,c,e) and the absence of diffraction patterns in SAED. The first crystallization sign was detected on day 3 of mineralization, as shown in Figure 4e. The result of SAED patterns did not show any diffraction one, which indicated that the minerals were still predominantly amorphous. However, the mineralization in Col-I fibrils only occurred at localized areas, which later mineralized in the lateral direction rather than along the fibrils in the day 7 of mineralization, as shown in Figure 4e,g,i. In contrast, Col-PDA fibrils exhibited heavy mineralization in 3 days, as shown in Figure 4f; in addition, the nearly complete mineralization of whole fibrils was obtained only after 2 days of mineralization (see later in Figure 6). After completion of intrafibrillar mineralization, the diameter of mineralized Col-PDA fibrils expanded over time due to mineral deposition (Figure S5). The diameter was measured as 83.8 ± 9.3 nm after a day, 107.2 ± 4.8 nm after 2 days, and 241 ± 15.6 nm after 3 days of incubation time for mineralization. Additionally, after 3 days of mineralization, HAp crystals grew entirely on the inner and outer surfaces of Col-PDA fibrils, and it was confirmed that the crystal growth in the bulk solution of m-SBF proceeded (see Figure 4f,h,j). It was proposed that in the presence of pAsp and PDA at the initial stage of mineralization, the gap and overlap zones, which are confined spaces for nucleation, minimize the surface area of the nuclei. As a new interface is created between the supersaturated solution and the crystal aggregate, particle agglomeration by the supersaturated solution into a stable crystalline phase is advantageous as more particles are added to the aggregate. The formation of ACP in the gap and overlap zones with Ca^{2+} and PO_4^{3-} ions attracted by PDA can be considered as a 2D confinement by the specific distance between Col-I molecules in Col-PDA fibrils. The confined regions inside Col-PDA fibrils can induce the decreased energy barrier. Recently, Kim et al. summarized the formation of a 2D crystal of uniform height (h) in a confined gap inside collagen.[4] The gap and overlap zones provide sites for nucleation as the space effectively reduces the interfacial energy term ($4\pi r^2\gamma \rightarrow 2rh\gamma$) by minimizing the effective surface area of the nucleus. As the gap and overlap zones now have a lower nucleation energy compared to the bulk solution with pAsp, nucleation inside the zones is more favorable over the extrafibrillar mineralization. Therefore, the extrafibrillar mineralization is rarely found at the partially intrafibrillar mineralization state, i.e., the early days of mineralization. The mineralization in Col-PDA exhibits a higher degree of mineralization, suggesting the promotion effect of mineralization with PDA in Col-I fibrils. Therefore, it can be concluded that PDA can enhance the biomimetic intrafibrillar mineralization of Col-I.

The pristine Col-I fibrils were highly aligned in the longitudinal dimension and disorderly twisted in the lateral dimension, as shown in Figure 5a. The disorder in the lateral dimension is caused by the lateral expansion of fibrils due to the imbibition of water molecules.[41,42] This phenomenon occurs temporarily during the initial mineralization stage and can be inferred by the infiltration of fluid-like ACP precursors via a polymer-induced liquid precursor process.[43] The Col-I fibrils can be penetrated by the amorphous mineral phase, i.e., ACP, with a higher electron density that appeared in a relatively darker contrast (Figure 5b). Upon the transformation of the amorphous to crystalline phase, excess water is progressively removed during the deposition of HAp within the Col-I fibrils.[44] This progressive dehydration process might have occurred in the Col-I fibrils, resuming their original dimensions as we can see in the higher contrast area. The mineral phase is predominantly amorphous, as indicated in the absence of any diffraction pattern from the result of SAED, as shown in Figure 5c. It is suggested that the electron density, which provides a darker contrast, originates from either ACP or the thickness contrast of twisted fibrils. The former is much

https://doi.org/10.1021/acsomega.1c05198
ACS Omega 2022, 7, 4821−4831

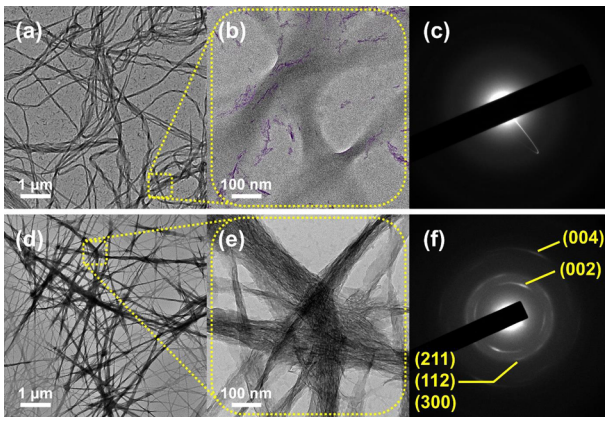

Figure 5. For a day, TEM images and SAED patterns of the mineralized (a–c) pristine Col-I and (d–f) Col-PDA fibrils. (a, b) No intrafibrillar mineralization was found for the pristine Col-I fibrils, while there was formation of precipitated particles all over the carbon film TEM grid. Particles in (b) magnified image are colored in purple. (c) SAED pattern shows the absence of any diffraction patterns of HAp. (d, e) The Col-PDA fibrils were partially mineralized and (f) the SAED patterns show the arc-shaped reflection of the mineral phase HAp.

more feasible in this study. However, even with the presence of pAsp, there was formation of precipitated particles observed at this mineralization stage. When the extrafibrillar mineralization has a much higher nucleation energy barrier, then intrafibrillar mineralization would be thus preferred. In Col-PDA, the ACPs that infiltrated in fibrils were mineralized, as ACP transformed to HAp in 24 h of mineralization (Figure 5d–f). The mineral phase inside the fibrils can be indicated as a darker contrast. The darker contrast area revealed the bundles of needle-like mineral strands associated in Col-I fibrils oriented longitudinally along with the fibrils, which referred to an intrafibrillar mineralization. As such, many of the charged amino acid sites correspond to the known Col-I gaps and overlap zones. Once nucleation occurs at a given site, an individual nuclei would recruit additional Ca^{2+} and PO_4^{3-} ions to grow into a crystal by adsorbing and/or incorporating ions, each bound to the charged amino acid residues neighboring the growing crystal. More specifically, lysine and arginine that are both located at the gap and overlap zone could be bound with PO_4^{3-}. Further, the combination of these positively charged residues with the presence of negatively charged glutamic or aspartic acid residues would create a pocket, in which both Ca^{2+} and PO_4^{3-} ions could be accommodated.[45,46] Additionally, the confined gap spaces' geometry within Col-I fibrils also lead to the crystal growth along the long axis of the fibrils. The SAED pattern of mineralized Col-I fibrils confirmed that the mineral phase was crystalline HAp. The (002) diffraction plane is an arc-shaped reflection, which is indicative of the oriented *c*-axis of HAp

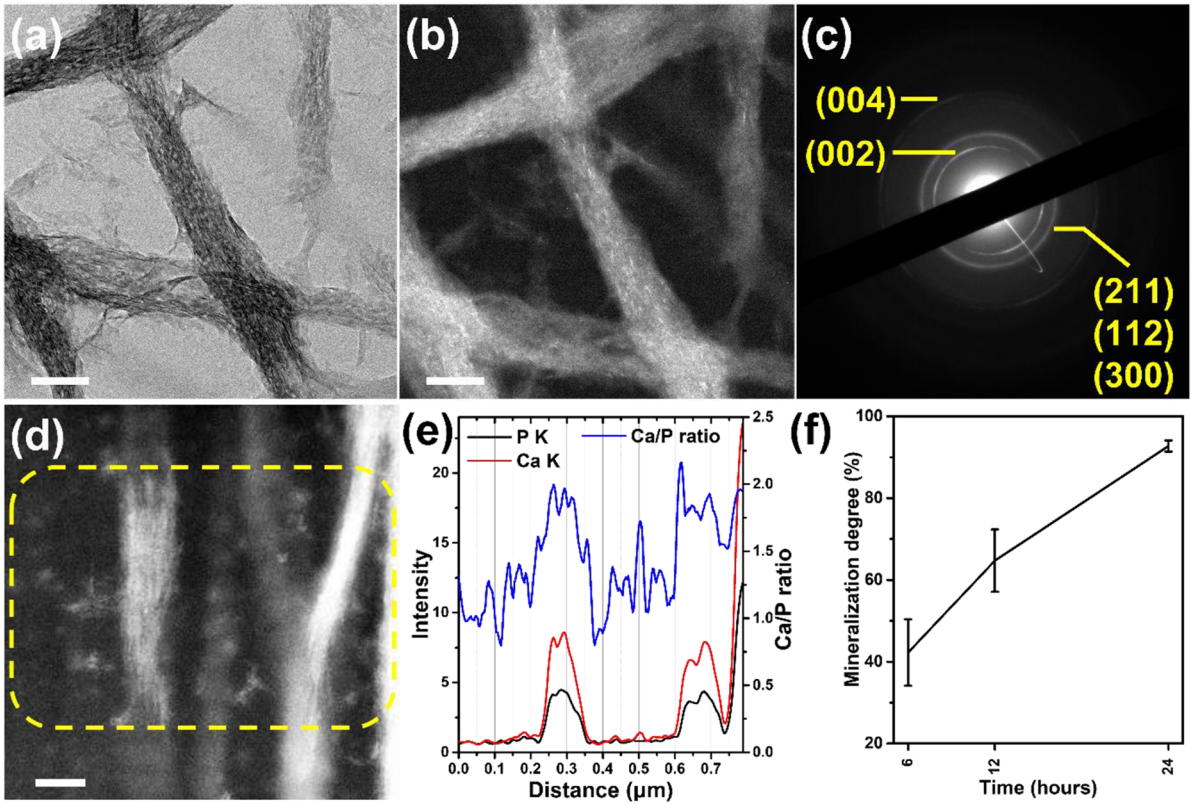

Figure 6. (a–e) Mineralization of the Col-PDA fibrils for a day. (a) Bright-field TEM image of Col-I fibrils showing the partially mineralized ones. (b) Dark-field TEM image of Col-I fibrils after mineralization constructed by selecting one of the (002) arcs with the objective aperture. It illuminates some of the [001] aligned HAp crystals, which appeared as short bright strands. (c) SAED pattern of mineralized Col-I fibrils in (a) with labeled lattice planes of HAp. Electron diffraction of the fibrils demonstrates that the crystals are oriented with their *c*-axis parallel to the direction of the fibrils. (d, e) Elemental mapping analysis of mineralized Col-PDA (scale bars: 100 nm). (f) Results of calculating the mineralization degree by quantifying the mineralized area based on the Col-I fibril area by choosing the threshold (n = 4). Col-PDA indicated the mineralization degree that advanced at the Col-I fibril area as the mineralization time increases.

https://doi.org/10.1021/acsomega.1c05198
ACS Omega 2022, 7, 4821–4831

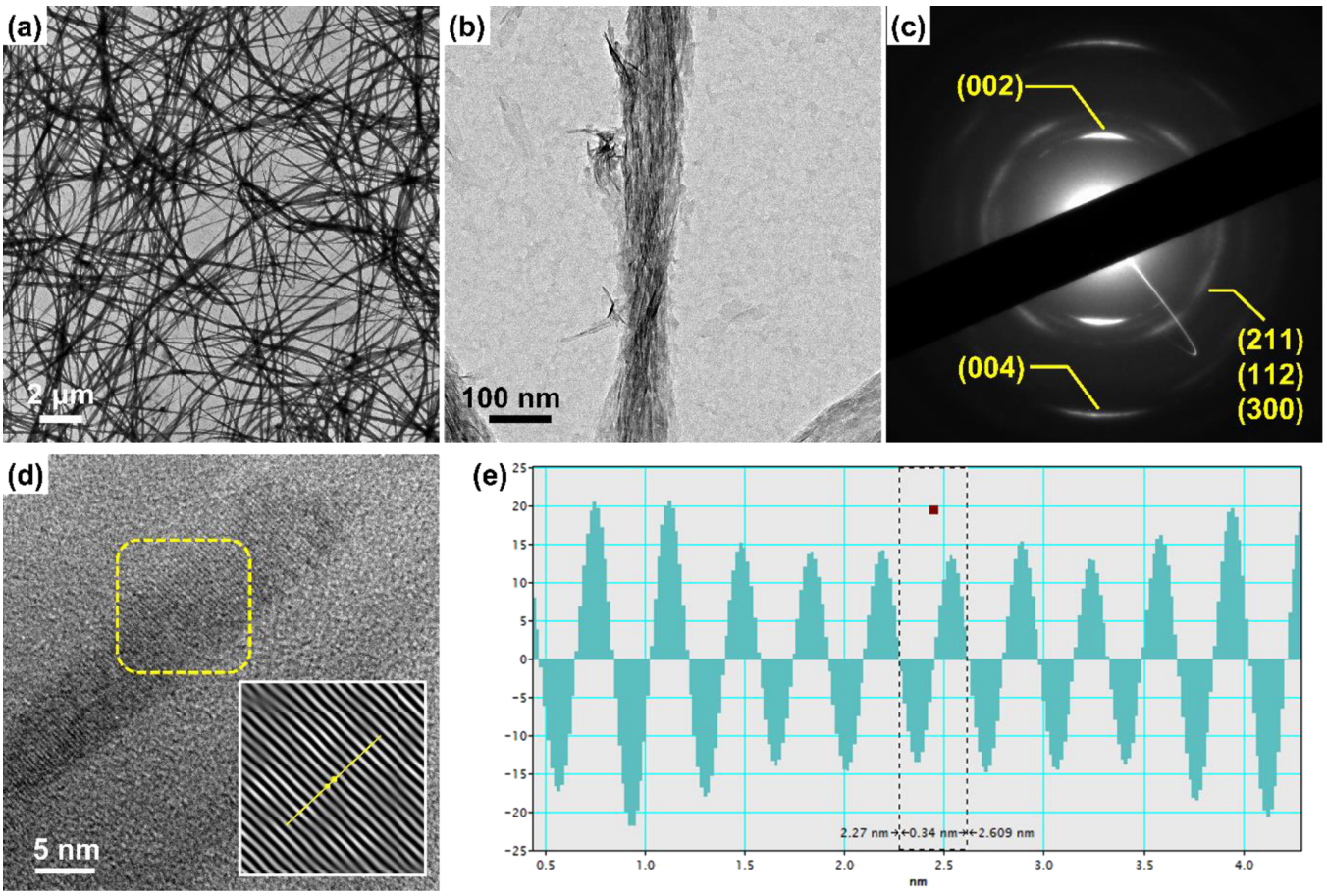

Figure 7. TEM results of mineralized Col-PDA fibrils for 2 days. (a, b) TEM images of the nearly complete mineralized Col-PDA fibrils. (c) SAED patterns of HAp crystals in the mineralized Col-PDA fibrils. (d) HRTEM images of mineralized Col-PDA fibrils for 2 days. HRTEM lattice analysis images indicate an interplanar spacing of 0.34 nm, which is consistent with the HAp lattice plane of the (002) and filtered inverse-FFT image reconstructed by spatial frequencies from the yellow box region. (e) Corresponding line profiles of the lattice plane (002) from (d).

along with the longitudinal axis of the Col-I fibrils, which agreed with the mineralized fibrils in natural bone tissue. The (211), (112), and (300) diffraction planes are close to each other, producing a thicker and apparently continuous diffused rings related to their three lattice spacings of d = 2.814, 2.778, and 2.720 Å, respectively, as shown in Figure 5f.[47]

The partially mineralized Col-PDA fibrils were clearly observed in the bright-field TEM image, as shown in Figure 6a. The oriented c-axis of HAp crystallites was observed more clearly as bright streaks in the dark-field TEM image (see Figure 6b). The SAED patterns again confirmed that the mineral phase was HAp (Figure 6c). The (002) and (004) diffraction arches were followed by the alignment of c-axis needle-like minerals parallel to the fibrils. As shown in Figure S6, the elemental mapping in TEM indicated the uniform composition of the integration of the CaP mineral phase within the Col-PDA fibrils mineralized for 6, 12, and 24 h. The Ca/P atomic ratio of the needle-shaped HAp (1.425 ± 0.38) is similar to that of the natural bone tissue, as can be seen from the EDS line scanning profile (Figure 6d,e). The degree of mineralization was calculated by choosing the threshold in ImageJ software (National Institute of Health, Bethesda, MD, USA) by considering the contrast in the results of EDS mapping images (Figure S6), as shown in Figure 6f. DA polymerization during the collagen self-assembly process was a critical factor in intrafibrillar mineralization. We proposed that with the collagen self-assemble process, the introduced DA would possibly be located at the gap regions, specifically binding with primitive amide on lysine residues and at the n-terminate of collagen molecules, as illustrated in Figure 1. The catecholamine moieties that are abundant in PDA are indicated as a possibility for the nucleation of hydroxyapatite by co-precipitation of Ca^{2+} and PO_4^{3-}. The increase in the mineralization degree over time suggested the mineralization at the specific areas of Col-PDA fibrils.

The specific binding sites of PDA on Col-PDA fibrils were investigated by using Cy5 NHS ester, an amine-reactive red-emitting fluorescent dye. It was used to react with the free primary amine group (lysine residues), as shown in Figure S7. Both samples were prepared by drop-casting self-assembled fibrils on a TEM grid with the protocols presented in the Experimental Section and subsequently dying by Cy5 NHS ester. Each of the three images was taken at 0.5 ms exposure time with an Olympus Japan 800 × 600 image RGB camera at the different areas of the TEM grid of each sample of Col-I and Col-PDA fibrils. Figure S7 shows that for Col-I fibrils, the images showing red fluorescence indicate the existence of free amine ($-NH_2$) along the Col-I fibrils, while for Col-PDA fibrils, red emitted fluorescence is nearly absent. The absence of emitted fluorescence of Col-PDA can imply that due to the binding of PDA on $-NH_2$, there is less free amine to bond with Cy5 NHS ester. From this result, it can be demonstrated

https://doi.org/10.1021/acsomega.1c05198
ACS Omega 2022, 7, 4821−4831

that the preferred PDA binding site of Col fibrils is at the amine group. However, for the confined space at the gap and overlap region, this imaging technique still cannot confirm the location of PDA by a fluorescence dying method due to the limitation of the technique. The fluorescence intensity corresponding to the presence of free primary amines was further assessed by ImageJ software. For intensity calculation, one image of each sample of Col-I and Col-PDA fibrils was analyzed, and their average intensity, plotted in Figure S8, indicated a huge difference in the number of primary free amines before and after PDA. However, direct characterization evidence to prove the exact role and binding sites of PDA of the confined space at the gap and overlap region in the regulation of intrafibrillar mineralization still required further studies.

The mineralized Col-PDA fibrils for 2 days in m-SBF revealed the completely filled ones, with needle-like minerals shown in Figure 7a and a mineralized Col-PDA fibril in Figure 7b. Figure 7c shows the aligned needle-like minerals along with the fibrils as the arc-shaped diffraction rings of (002) and (004). The HRTEM lattice image clearly shows the growth direction of HAp along with the (002) interplanar spacing of approximately 0.34 nm, as shown in Figure 7d. The filtered inverse fast Fourier transform (FFT) of the HRTEM image, as shown in Figure 7e, was applied for highly precise measurements of the lattice spacing. The measured *d*-spacing was 0.34 nm. It shows excellent agreement with the lattice contrast of the (002) plane, which is known as the basal plane of hexagonal HAp. As mentioned earlier, the HRTEM lattice images and SAED patterns of Col-PDA mineralization obviously showed the high-quality crystalline phase of HAp, which was in contradiction with the broad peak from the XRD results even up to 8 days of mineralization of Col-PDA. It can be explained by the fact that the Col-PDA fibril specimens for TEM studies were prepared as an almost single layer of fibril, while the larger amount of prepared Col-PDA fibrils for XRD is likely to form hydrogel-like specimens after the centrifugation process in the washing step before mineralization. The rate of mineralization could be affected by the diffusion rate of ions that is dependent on the pore size and porosity of the hydrogel-like Col-PDA fibrils' structure. Therefore, the mineralization of Col-PDA in XRD results showed a much slower kinetics than that in TEM results.

Numerous experimental studies and theoretical simulations have been performed to understand the mechanisms of induced or controlled mineralization in the collagen matrix. Unlike the conventional nucleation step that is generally known from a thermodynamic point of view, the intrafibrillar mineralization of Col-PDA involves ACP, which would be a metastable solid phase, and can be interpreted as a multi-step process via ACP. The nucleation of the stable phase within the Col-PDA fibrils leads to repeated dissolution or recrystallization of the metastable phase, eventually leading to heterogeneous mineralization on the metastable particle. It is consistent with the Ostwald step rule mentioned in the Introduction. Basically, there are many non-uniformly charged or uncharged amino acids in the gap and overlap zones between Col-I molecules in Col-I fibrils. The abovementioned ACP is non-uniformly present in intrafibrillar Col-PDA by PDA, calcium, and phosphate ions combined with these amino acids. In this study, it was confirmed that PDA induced by adsorption to Col-I fibrils bound not only to the Col-I gap zone (terminal regions of tropocollagen formed by procollagen peptidase) but also to the overlap zone, influencing the regular arrangement of Col-I molecules and thus the intrafibrillar mineralization. Unlike the case of using only pAsp, which is used for mineralization of Col-I fibrils, in fibrils with PDA, the degree of intrafibrillar mineralization was increased. pAsp, known as an extrafibrillar nucleation inhibitor, increases the interfacial energy between the nucleus in the m-SBF solution.[48] On the other hand, PDA added to confined regions such as the gap and overlap zones of intrafibrillar Col-PDA reduces the reactive surface area of the nucleus, lowering the energy barrier and reducing the surface energy. It also appears to be due to the high affinity and stable and efficient adsorption in between the Col-I fibrils and PDA. Compared to pristine Col-I fibrils, Col-PDA fibrils can increase the contact area between Col-PDA fibrils and ACP by highly hydrophilic PDA, thereby lowering the energy barrier for ACP to deposit on Col-PDA fibrils.[29] Thus, PDA could be shown to enhance ACP nucleation in Col-PDA fibrils and subsequent intrafibrillar mineralization. PDA had an impact on having a rigid lamellar structure that acted as a support in actual bone tissue. In addition, PDA enhances not only the *d*-spacing arrangement, which regularly composed the Col-I fibrils but also the hydroxyl group by binding to the side of the molecules. As this increased hydroxyl group influences the provision of ACP binding sites, it can be concluded that Col-PDA fibrils exhibit a rapid rate of mineralization. As a conclusion, Figure 8 schematically shows the biomimetic intrafibrillar mineralization with the functionalization of PDA.

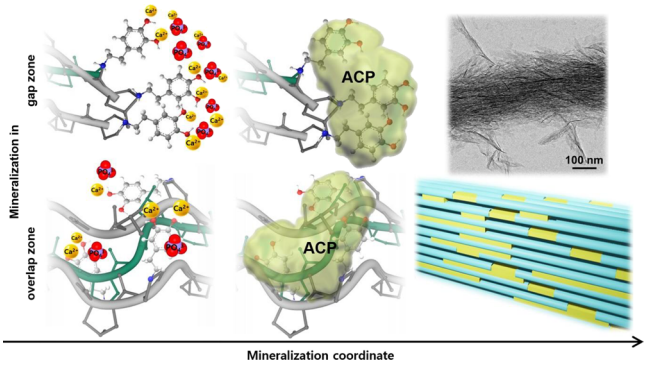

Figure 8. The gap zone and overlap zone between Col-I molecules that are regularly arranged, and PDA bound to the surface of the Col-I molecule attracts Ca^{2+} and PO_4^{3-} ions to induce ACP nucleation in Col-I fibrils. In contrast to pristine Col-I fibrils, which preferentially undergo ACP nucleation and mineralization in the extrafibrillar regions rather than the intrafibrillar gap zone, Col-PDA fibrils preferentially undergo ACP nucleation and mineralization in several sites of the intrafibrillar gap zones. Compared to the energy required for the mineralization process in the extrafibrillar regions, the ACP nuclei present in the intrafibrillar specifically sized space have an immense impact on the intrafibrillar mineralization by reducing the surface area exposed to the outside.

3. CONCLUSIONS

PDA, a functional polymer, was applied in the process of self-assembly of Col-I to improve the intrafibrillar mineralization. The polymerized DA (PDA) and DA applied in the Col-I self-assembly process resulted in a markedly improved mineralization. The PDA binding to the collagen molecules reduced the interfacial energy between the collagen and ACP. Therefore, the liquid-like ACP is more obviously likely to enter to Col-I

https://doi.org/10.1021/acsomega.1c05198
ACS Omega 2022, 7, 4821−4831

fibrils specifically at the gap and overlap zones, which we proposed as possible binding sites for PDA. The ACP at the early stage of mineralization induced the appearance of a cross-banding pattern. TEM results confirmed that the mineral contents in the Col-PDA fibrils were significantly enhanced by the intrafibrillar mineralization by dragging the liquid-like precursors into the collagen. After complete mineralization, needle-like HAp was found in the fibrils. The (002) diffraction plane of HAp is an arc-shaped reflection, which is indicative of the oriented *c*-axis of HAp along with the longitudinal axis of the Col-I fibrils, which agreed with the Col-I fibrils in natural bone tissue. Therefore, our presented work here would be one of potential platforms for the preparation of collagen tissue engineering scaffolds for future development of mineralized biomaterials by providing insights into the intrafibrillar mineralization.

4. EXPERIMENTAL SECTION

4.1. Materials. Poly(L-aspartic acid sodium salt) (pAsp, 27 kDa) was purchased from ALAMANDA Polymers (Huntsville, AL, USA). Acid-soluble Col-I from the rat tail was purchased from Corning (Bedford, MA, USA). Calcium chloride ($CaCl_2$), disodium phosphate (Na_2HPO_4), sodium chloride (NaCl), dopamine hydrochloride (DA, $C_8H_{11}NO_2$·HCl), glycine ($C_2H_5NO_2$), potassium chloride (KCl), sodium azide (NaN_3), and cyanine-5 NHS ester (Cy5 NHS ester) were all purchased from Sigma-Aldrich (St. Louis, MO, USA). Tris-HCl (1 M, pH 8.5) was purchased from CureBio (Seoul, South Korea). Uranyl acetate was purchased from SPI Supplies (West Chester, PA, USA). Deionized water was autoclaved prior to use.

4.2. Self-Assembly of Collagen Fibrils. Assembling buffer solutions for the self-assembly of Col-I fibrils were prepared with 50 mM glycine and 200 mM KCl in DI water, and the pH was pre-adjusted to 9.2 with 1 M NaOH as described by Shao et al.[23] (1) For the pristine collagen fibrils, to assemble Col-I, the stock solution of Col-I from the rat tail tendon was dropped to the assembling buffer solution resulting in 50 μg/mL, and it was incubated at 37 °C for 12 h. To confirm the periodical structure constituted by the self-assembly process, the Col-I fibrils were negatively stained with 1% uranyl acetate for 15 s for TEM. (2) For the collagen fibrils with dopamine polymerization, 10 μM DA solution to be added during the Col-I self-assembly process was prepared with 10 mM Tris-HCl buffer with pH 8.5 as a solvent. The weight ratios of Col-I and DA were set to 5:4, 5:8, 5:16, 1:8, 1:16, and 1:32, which are best suited for the collagen fibrosis and mineralization process (Table S1). After mixing the prepared DA solution and the assembling buffer, Col-I was immediately added to DA in the set ratios and incubated at 37 °C for 12 h.

4.3. Mineralization of Collagen with Polydopamine. Modified simulated body fluid (m-SBF) was prepared separately as calcium and phosphate stock solutions.[49] The calcium stock solution was prepared by dissolving 3.34 mM $CaCl_2$ in DI water. The phosphate stock solution was prepared by dissolving 19 mM Na_2HPO_4 and 300 mM NaCl in DI water. A 0.37 M pAsp solution was mixed with the prepared calcium stock solution with the final concentration of pAsp in 0.566 mg/mL. After that, the phosphate stock solution was mixed with the calcium stock solution with dissolved pAsp in the same volume ratio of calcium and phosphate stock solutions. Then, 5% NaN_3 was added to the mineralization solution and mixed quickly to retard bacterial growth. All samples in the m-SBF were sealed to control the evaporation rate and incubated at a constant temperature of 37 °C for a designated time. The mineralized solutions were freshly changed every 24 h.

4.4. Material Properties of Mineralized Collagen Fibrils. Circular dichroism (CD) spectroscopy was used to confirm the triple helix and random coil morphology before and after the formation of self-assembled Col-I fibrils. Self-assembled Col-I and Col-PDA fibrils were both prepared with the same protocols as described earlier in the Self-Assembly of Collagen Fibrils Section at the final concentration of Col-I of 50 μg/mL in the assembling buffer and DA Tris-HCl mixed assembling buffer solutions. Both solutions were added in a quartz cuvette and incubated at 37 °C for 12 h. X-ray diffraction (XRD) and Fourier-transform infrared (FTIR) spectroscopy analysis were performed to observe changes in the material properties of the self-assembled collagen, DA-conjugated collagen, and mineralized collagen. The self-assembled Col-I fibrils with and without DA for these measurements were prepared with the same methods as described in the Self-Assembly of Collagen Fibrils Section with a larger final volume of solution at 50 mL to obtain enough fibrils for characterization. After incubation for 12 h, the assembling buffer was removed from all samples by centrifugation at 4000 rpm for 15 min and washed three times using autoclaved DI water. To quantify the free amine before and after DA was added to collagen, the drop-cast fibrils on TEM grids were dyed by Cy5 NHS ester for 2 h. The mineralization process was further conducted by adding the prepared m-SBF solution from the Mineralization of Collagen with Polydopamine Section to Col-I and Col-PDA fibrils and then incubating at 37 °C for 3 and 7 days. Mineralized Col and Col-PDA were centrifuged at 4000 rpm for 15 min to remove m-SBF solution and washed three times with autoclaved DI water. All samples were immediately quenched with liquid nitrogen and lyophilized for at least 24 h before XRD and FTIR measurement.

■ ASSOCIATED CONTENT

Supporting Information

The Supporting Information is available free of charge at https://pubs.acs.org/doi/10.1021/acsomega.1c05198.

Table of the DA concentration series added during the self-assembly process; TEM images of Col-I fibrils negatively stained by uranyl acetate; AFM images of Col-PDA fibrils with a series of different added DA concentrations; CD results of the Col-I molecule structure before and after self-assembly with polymerization of DA; EDS mapping results of pristine Col-I and Col-PDA fibrils mineralized for 12 h; fluorescence images of Cy5 NHS ester-labeled Col-I and Col-PDA fibrils; and mean fluorescence intensity (PDF)

■ AUTHOR INFORMATION

Corresponding Authors

Sang Ho Oh − *Department of Energy Science, Sungkyunkwan University, Suwon 16419, Republic of Korea*; Email: sanghooh@skku.edu

Min-Ho Hong − *Nature Inspired Materials Processing Research Center, Department of Energy Science, Sungkyunkwan University, Suwon 16419, Republic of Korea;*

https://doi.org/10.1021/acsomega.1c05198
ACS Omega 2022, 7, 4821−4831

Present Address: Department of Dental Biomaterials and Research Institute of Oral Science, College of Dentistry, Gangneu ng-Wonju National University, Gangneung 25457, Republic of Korea (M.-H.H.); orcid.org/0000-0001-9268-9906; Email: mhong@gwnu.ac.kr

Hyunjung Shin − *Nature Inspired Materials Processing Research Center, Department of Energy Science, Sungkyunkwan University, Suwon 16419, Republic of Korea;* orcid.org/0000-0003-1284-9098; Email: hshin@skku.edu

Authors

Urasawadee Amornkitbamrung − *Nature Inspired Materials Processing Research Center, Department of Energy Science, Sungkyunkwan University, Suwon 16419, Republic of Korea*

Yongjae In − *Nature Inspired Materials Processing Research Center, Department of Energy Science, Sungkyunkwan University, Suwon 16419, Republic of Korea*

Zhen Wang − *Department of Energy Science, Sungkyunkwan University, Suwon 16419, Republic of Korea*

Jiyoon Song − *Nature Inspired Materials Processing Research Center, Department of Energy Science, Sungkyunkwan University, Suwon 16419, Republic of Korea*

Complete contact information is available at: https://pubs.acs.org/10.1021/acsomega.1c05198

Notes

The authors declare no competing financial interest.

■ ACKNOWLEDGMENTS

This research was supported by the National Research Foundation of Korea (NRF) grants funded by the Ministry of Science and ICT under contract NRF-2018M3C1B7021994 (Bioinspired Innovation Technology Development Project) and the Ministry of Education contract NRF-2020R1I1A1A01070982 (Basic Science Research Program).

■ REFERENCES

(1) Qin, Z.; Gautieri, A.; Nair, A. K.; Inbar, H.; Buehler, M. J. Thickness of hydroxyapatite nanocrystal controls mechanical properties of the collagen−hydroxyapatite interface. *Langmuir* **2012**, *28*, 1982−1992.

(2) Nair, A. K.; Gautieri, A.; Chang, S.-W.; Buehler, M. J. Molecular mechanics of mineralized collagen fibrils in bone. *Nat. Commun.* **2013**, *4*, 1724.

(3) Nair, A. K.; Gautieri, A.; Buehler, M. J. Role of intrafibrillar collagen mineralization in defining the compressive properties of nascent bone. *Biomacromolecules* **2014**, *15*, 2494−2500.

(4) Kim, D.; Lee, B.; Thomopoulos, S.; Jun, Y.-S. The role of confined collagen geometry in decreasing nucleation energy barriers to intrafibrillar mineralization. *Nat. Commun.* **2018**, *9*, 962.

(5) Engstrom, A. Apatite-collagen organization in calcified tendon. *Exp. Cell Res.* **1966**, *43*, 241.

(6) White, S. W.; Hulmes, D. J.; Miller, A.; Timmins, P. A. Collagen−mineral axial relationship in calcified turkey leg tendon by X-ray and neutron diffraction. *Nature* **1977**, *266*, 421−425.

(7) Robinson, R.; Watson, M. Collagen-crystal relationships in bone as seen in the electron microscope. *Anat. Rec.* **1952**, *114*, 383−409.

(8) Höhling, H.; Barckhaus, R.; Krefting, E. Hard tissue formation in collagen-rich systems: calcium phosphate nucleation and organic matrix. *Trends Biochem. Sci.* **1980**, *5*, 8−11.

(9) Weiner, S.; Traub, W. Crystal size and organization in bone. *Connect. Tissue Res.* **1989**, *21*, 259−265.

(10) Ziv, V.; Sabanay, I.; Arad, T.; Traub, W.; Weiner, S. Transitional structures in lamellar bone. *Microsc. Res. Tech.* **1996**, *33*, 203−213.

(11) Fernandez-Moran, H.; Engström, A. Ultrastructural organization of bone. *Nature* **1956**, *178*, 494−495.

(12) He, K.; Sawczyk, M.; Liu, C.; Yuan, Y.; Song, B.; Deivanayagam, R.; Nie, A.; Hu, X.; Dravid, V. P.; Lu, J. Revealing nanoscale mineralization pathways of hydroxyapatite using in situ liquid cell transmission electron microscopy. *Sci. Adv.* **2020**, *6*, No. eaaz7524.

(13) Posner, A. S.; Betts, F. Synthetic amorphous calcium phosphate and its relation to bone mineral structure. *Acc. Chem. Res.* **1975**, *8*, 273−281.

(14) Boonrungsiman, S.; Gentleman, E.; Carzaniga, R.; Evans, N. D.; McComb, D. W.; Porter, A. E.; Stevens, M. M. The role of intracellular calcium phosphate in osteoblast-mediated bone apatite formation. *Proc. Natl. Acad. Sci. U. S. A.* **2012**, *109*, 14170−14175.

(15) Iwayama, T.; Okada, T.; Ueda, T.; Tomita, K.; Matsumoto, S.; Takedachi, M.; Wakisaka, S.; Noda, T.; Ogura, T.; Okano, T. Osteoblastic lysosome plays a central role in mineralization. *Sci. Adv.* **2019**, *5*, No. eaax0672.

(16) Nudelman, F.; Pieterse, K.; George, A.; Bomans, P. H. H.; Friedrich, H.; Brylka, L. J.; Hilbers, P. A. J.; de With, G.; Sommerdijk, N. A. J. M. *Nat. Mater.* **2010**, *9*, 1004−1009.

(17) Song, Q.; Jiao, K.; Tonggu, L.; Wang, L.; Zhang, S.; Yang, Y.; Zhang, L.; Bian, J.; Hao, D.; Wang, C. Contribution of biomimetic collagen-ligand interaction to intrafibrillar mineralization. *Sci. Adv.* **2019**, *5*, No. eaav9075.

(18) Deshpande, A. S.; Beniash, E. Bioinspired synthesis of mineralized collagen fibrils. *Cryst. Growth Des.* **2008**, *8*, 3084−3090.

(19) Qi, Y.; Ye, Z.; Fok, A.; Holmes, B. N.; Espanol, M.; Ginebra, M.-P.; Aparicio, C. Effects of molecular weight and concentration of poly (acrylic acid) on biomimetic mineralization of collagen. *ACS Biomater. Sci. Eng.* **2018**, *4*, 2758−2766.

(20) Chen, J.; Burger, C.; Krishnan, C. V.; Chu, B.; Hsiao, B. S.; Glimcher, M. J. In vitro mineralization of collagen in demineralized fish bone. *Macromol. Chem. Phys.* **2005**, *206*, 43−51.

(21) Kim, Y. K.; Gu, L.-s.; Bryan, T. E.; Kim, J. R.; Chen, L.; Liu, Y.; Yoon, J. C.; Breschi, L.; Pashley, D. H.; Tay, F. R. Mineralisation of reconstituted collagen using polyvinylphosphonic acid/polyacrylic acid templating matrix protein analogues in the presence of calcium, phosphate and hydroxyl ions. *Biomaterials* **2010**, *31*, 6618−6627.

(22) Tsai, S.-W.; Hsu, F.-Y.; Chen, P.-L. Beads of collagen−nanohydroxyapatite composites prepared by a biomimetic process and the effects of their surface texture on cellular behavior in MG63 osteoblast-like cells. *Acta Biomater.* **2008**, *4*, 1332−1341.

(23) Shao, C.; Zhao, R.; Jiang, S.; Yao, S.; Wu, Z.; Jin, B.; Yang, Y.; Pan, H.; Tang, R. Citrate improves collagen mineralization via interface wetting: a physicochemical understanding of biomineralization control. *Adv. Mater.* **2018**, *30*, 1704876.

(24) Qu, Y.; Gu, T.; Du, Q.; Shao, C.; Wang, J.; Jin, B.; Kong, W.; Sun, J.; Chen, C.; Pan, H.; Tang, R.; Gu, X. Polydopamine Promotes Dentin Remineralization via Interfacial Control. *ACS Biomater. Sci. Eng.* **2020**, *6*, 3327−3334.

(25) Ryu, J.; Ku, S. H.; Lee, H.; Park, C. B. Mussel-inspired polydopamine coating as a universal route to hydroxyapatite crystallization. *Adv. Funct. Mater.* **2010**, *20*, 2132−2139.

(26) Wang, Z.; Yang, H.-C.; He, F.; Peng, S.; Li, Y.; Shao, L.; Darling, S. B. Mussel-inspired surface engineering for water-remediation materials. *Matter* **2019**, *1*, 115−155.

(27) Yang, Z.; Liu, M.; Yang, Y.; Zheng, M.; Liu, X.; Tan, J. Biofunctionalization of zirconia with cell-adhesion peptides via polydopamine crosslinking for soft tissue engineering: effects on the biological behaviors of human gingival fibroblasts and oral bacteria. *RSC Adv.* **2020**, *10*, 6200−6212.

(28) Wu, C.; Han, P.; Liu, X.; Xu, M.; Tian, T.; Chang, J.; Xiao, Y. Mussel-inspired bioceramics with self-assembled Ca-P/polydopamine composite nanolayer: preparation, formation mechanism, improved

cellular bioactivity and osteogenic differentiation of bone marrow stromal cells. *Acta Biomater.* **2014**, *10*, 428−438.
(29) Cheng, Y.-L.; Chen, Y.-W.; Wang, K.; Shie, M.-Y. Enhanced adhesion and differentiation of human mesenchymal stem cell inside apatite-mineralized/poly (dopamine)-coated poly (ε-caprolactone) scaffolds by stereolithography. *J. Mater. Chem. B* **2016**, *4*, 6307−6315.
(30) Zhou, Y.-Z.; Cao, Y.; Liu, W.; Chu, C. H.; Li, Q.-L. Polydopamine-induced tooth remineralization. *ACS Appl. Mater. Interfaces* **2012**, *4*, 6901−6910.
(31) Leow, W. W.; Hwang, W. Epitaxially guided assembly of collagen layers on mica surfaces. *Langmuir* **2011**, *27*, 10907−10913.
(32) Leikin, S.; Rau, D.; Parsegian, V. Temperature-favoured assembly of collagen is driven by hydrophilic not hydrophobic interactions. *Nat. Struct. Biol.* **1995**, *2*, 205−210.
(33) Krimm, S.; Bandekar, J. Vibrational spectroscopy and conformation of peptides, polypeptides, and proteins. *Adv. Protein Chem.* **1986**, *38*, 181−364.
(34) Zhu, S.; Gu, Z.; Xiong, S.; An, Y.; Liu, Y.; Yin, T.; You, J.; Hu, Y. Fabrication of a novel bio-inspired collagen−polydopamine hydrogel and insights into the formation mechanism for biomedical applications. *RSC Adv.* **2016**, *6*, 66180−66190.
(35) Kong, J.; Yu, S. Fourier transform infrared spectroscopic analysis of protein secondary structures. *Acta Biochim. Biophys. Sin.* **2007**, *39*, 549−559.
(36) Bandekar, J. Amide modes and protein conformation. *Biochim. Biophys. Acta* **1992**, *1120*, 123−143.
(37) Miyazawa, T.; Shimanouchi, T.; Mizushima, S. I. Characteristic infrared bands of monosubstituted amides. *J. Chem. Phys.* **1956**, *24*, 408−418.
(38) Saska, S.; Teixeira, L. N.; de Oliveira, P. T.; Gaspar, A. M. M.; Ribeiro, S. J. L.; Messaddeq, Y.; Marchetto, R. Bacterial cellulose-collagen nanocomposite for bone tissue engineering. *J. Mater. Chem.* **2012**, *22*, 22102−22112.
(39) Li, X.; Zou, Q.; Chen, H.; Li, W. In vivo changes of nanoapatite crystals during bone reconstruction and the differences with native bone apatite. *Sci. Adv.* **2019**, *5*, No. eaay6484.
(40) Nellist, P. D.; Pennycook, S. J. The principles and interpretation of annular dark-field Z-contrast imaging. *Adv. Imaging Electron Phys.* **2000**, *113*, 147−203.
(41) Hulmes, D. J.; Wess, T. J.; Prockop, D. J.; Fratzl, P. Radial packing, order, and disorder in collagen fibrils. *Biophys. J.* **1995**, *68*, 1661−1670.
(42) Svendsen, K. H.; Koch, M. H. X-ray diffraction evidence of collagen molecular packing and cross-linking in fibrils of rat tendon observed by synchrotron radiation. *EMBO J.* **1982**, *1*, 669−674.
(43) Gower, L. B. Biomimetic model systems for investigating the amorphous precursor pathway and its role in biomineralization. *Chem. Rev.* **2008**, *108*, 4551−4627.
(44) Chesnick, I. E.; Mason, J. T.; Giuseppetti, A. A.; Eidelman, N.; Potter, K. Magnetic resonance microscopy of collagen mineralization. *Biophys. J.* **2008**, *95*, 2017−2026.
(45) Silver, F. H.; Landis, W. J. Deposition of apatite in mineralizing vertebrate extracellular matrices: A model of possible nucleation sites on type I collagen. *Connect. Tissue Res.* **2011**, *52*, 242−254.
(46) Xue, Z.; Yang, M.; Xu, D. Nucleation of biomimetic hydroxyapatite nanoparticles on the surface of type I collagen: molecular dynamics investigations. *J. Phys. Chem. C* **2019**, *123*, 2533−2543.
(47) In, Y.; Amornkitbamrung, U.; Hong, M.-H.; Shin, H. On the Crystallization of Hydroxyapatite under Hydrothermal Conditions: Role of Sebacic Acid as an Additive. *ACS Omega* **2020**, *5*, 27204−27210.
(48) Habraken, W. J. E. M.; Tao, J.; Brylka, L. J.; Friedrich, H.; Bertinetti, L.; Schenk, A. S.; Verch, A.; Dmitrovic, V.; Bomans, P. H. H.; Frederik, P. M.; Laven, J.; van der Schoot, P.; Aichmayer, B.; de With, G.; DeYoreo, J. J.; Sommerdijk, N. A. J. M. Ion-association complexes unite classical and non-classical theories for the biomimetic nucleation of calcium phosphate. *Nat. Commun.* **2013**, *4*, 1507.
(49) Yao, S.; Xu, Y.; Shao, C.; Nudelman, F.; Sommerdijk, N. A.; Tang, R., A biomimetic model for mineralization of type-I collagen fibrils. In *Collagen*; Springer, 2019, pp. 39−54.

https://doi.org/10.1021/acsomega.1c05198
ACS Omega 2022, 7, 4821−4831